ACS OMEGA

Open Access

This article is licensed under CC-BY-NC-ND 4.0

http://pubs.acs.org/journal/acsodf

Article

# Electrocatalytic Degradation of Rhodamine B on the Sb-Doped $SnO_2$/Ti Electrode in Alkaline Medium

Dongli Deng, Ying Li,* Mingzhu Wu, Yang Song, Qiongjian Huang, Yiqin Duan, Yu Chang, Yangyang Zhao, and Chunling He

Cite This: *ACS Omega* 2023, 8, 48480−48490

Read Online

ACCESS | Metrics & More | Article Recommendations | Supporting Information

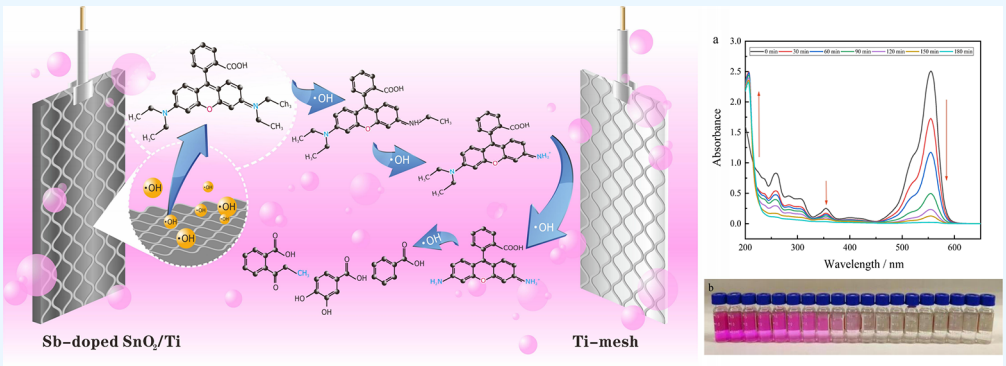


**ABSTRACT:** To realize efficient electrocatalytic degradation of organic compounds in alkaline wastewater, an Sb-doped $SnO_2$/Ti electrode was fabricated and employed for the removal of Rhodamine B (RhB), and the electrocatalytic oxidation performance of this electrode was assessed in an alkaline medium. In an alkaline solution (pH 11), the complete fading of 50 mg·$L^{-1}$ RhB could be achieved after 150 min of degradation, the removal efficiency of the chemical oxygen demand reached 56.1% at 300 min, and the degradation process of RhB followed the pseudo-first-order kinetic model very well. Under the attack of hydroxyl radicals, partial RhB was degraded to low-molecular-weight organic acids through N-demethylation and the destruction of the conjugated chromophore. Various techniques including scanning electron microscopy, X-ray diffraction, X-ray photoelectron spectroscopy, and cycle voltammetry were used to examine the changes in the morphology and structure, as well as the activity of the Sb-doped $SnO_2$/Ti electrode before and after use. The Sb-doped $SnO_2$/Ti electrode could be reproduced in batches, and each electrode was reused up to eight times without a significant decrease in degradation ability; the leaching amount of antimony was significantly lower than the national emission standard. The electrocatalytic oxidation of the dye wastewater sample was also performed with the desired results, indicating that electrochemical oxidation is a very promising technology for the treatment of alkaline dye wastewater using a Sb-doped $SnO_2$/Ti electrode.

## 1. INTRODUCTION

Industrial wastewater originating from various production activities, such as printing and dyeing, pharmaceutical, coking, and petrochemical, has high chroma, pH value and toxicity, and poor biodegradability.[1] Among them, organic dye wastewater with aromatic ring structure and xenobiotic properties has attracted more attention in the past decades, since they are noxious, highly carcinogenic, and nonbiodegradable. Organic dyes can not only hinder the self-purification of water but also bring toxic effects on the food chain by directly poisoning aquatic organisms or disrupting biological processes through light infiltration, even at very low concentrations.[2] However, the traditional wastewater treatment methods, such as adsorption,[3] coagulation,[4] and membrane separation,[5] merely transfer these organics to a solid phase or result in secondary pollution, which brings about a great challenge to completely remove them and meet the treatment standards.[6,7] Therefore, efficient and sustainable treatment technologies are needed to purify organic dye wastewater for environmental protection. Due to high efficiency, fast reaction, and broad adaptability, the advanced oxidation processes (AOPs) can effectively degrade organic dyes and even completely mineralize them by using the generated active species.[8] As an "environment-friendly" AOP, electrocatalytic oxidation technology has the advantages of

Received: October 24, 2023
Revised: November 16, 2023
Accepted: November 22, 2023
Published: December 6, 2023

© 2023 The Authors. Published by American Chemical Society

simple equipment and operation, high efficiency without secondary pollution, and easy automation and combination with other treatment methods. Based on the excellent ability to generate reactive oxygen species, such as hydroxyl radical ($^{\cdot}OH$) on an anode surface, electrocatalytic oxidation technology has been identified as an efficient and potential method to remove organic dyes from wastewater.[9,10]

As a typical organic dye, Rhodamine B (RhB) can color the water even at very low concentrations (approximately 1.0 mg·$L^{-1}$), thus hindering the photosynthetic processes of aquatic organisms.[11] Moreover, RhB has been found to have potential carcinogenicity, teratogenicity, and mutagenicity, and is difficult to degrade in the natural environment.[12−14] In recent years, many studies have used RhB as the representative pollutant to investigate the treatment of organic dyes in wastewater and various anodes have been developed by boron-doped diamond (BDD),[15] dimensionally stable anodes (DSA),[16,17] $PbO_2$,[18−20] $SnO_2$,[16,21−24] and several new materials.[25−28] In these studies, the effectiveness of electro-oxidation for the degradation of RhB has been proven, but it should be noted that these electrocatalytic oxidation processes usually run under neutral or weakly acidic conditions and the degradation performance of RhB in alkaline medium is not satisfactory. Liu et al.[28] reported that the removal efficiency of RhB was only 10% at the initial pH of 9, which is significantly lower than 96% in acid medium (pH 3) using the carbon nanotubes (CNTs)/agarose (AG) membrane on the ITO (indium tin oxide) electrode. Afterward, a similar phenomenon was also found in the study of Wu et al.,[19] and they prepared a $PbO_2$/Sb-$SnO_2$/$TiO_2$ nanotube arrays electrode to degrade RhB, and the removal efficiency of RhB in alkaline medium (pH 11) was 66.8%, corresponding to that of 99.7% in neutral medium. However, alkaline organic wastewater is ineluctable. In addition to the dye wastewater, some coking wastewater and pharmaceutical wastewater are also alkaline. Adjusting the initial pH before electro-oxidation treatment will consume a large amount of acid and increase the salinity of wastewater, which is neither economical nor technically feasible. Moreover, the pH of the aqueous phase can significantly affect the degradation of pollutants, the selectivity of reactions, and the stability of electrodes.[29,30] Therefore, it is of great significance to improve the degradation efficiency of RhB in an alkaline medium by electrocatalytic oxidation technology.

The practical feasibility of electro-oxidation technology for wastewater treatment requires the development of low-cost anodes with enough activity and stability. Compared with expensive BDD and gold electrodes, the lead-leaching risky $PbO_2$-based electrode, and complicated composite electrodes, the anode based on $SnO_2$−Sb is considered as the most promising alternative with the advantages of low cost, simple preparation, and high ability to generate hydroxyl radicals.[31,32] Based on the above considerations, we studied the electrocatalytic degradation of RhB in alkaline medium using Sb-doped $SnO_2$ coated on a titanium mesh electrode (Sb-doped $SnO_2$/Ti electrode). The degradation kinetic of RhB, the role of hydroxyl radicals in RhB elimination, the chemical oxygen demand (COD) removal, and the possible degradation pathways in the alkaline medium were investigated. The morphology and structure of this electrode before and after use in RhB degradation were characterized by various techniques and its electrochemical performance and stability in an alkaline degradation system were also examined. Moreover, the potential application of the Sb-doped $SnO_2$/Ti electrode for the degradation of the alkaline dye wastewater was demonstrated.

## 2. MATERIALS AND METHODS

**2.1. Regents and Materials.** All reagents and chemicals were of analytical grade unless stated otherwise. Rhodamine B (RhB), antimony oxide, stannous chloride dihydrate, and 2,5-dihydroxybenzoic acid were purchased from Adamas Reagent Co., Ltd., China. Acetic acid and methanol (HPLC grade) were supplied by Sigma-Aldrich (USA), and other reagents were purchased from Chengdu Kelong Chemical Reagent Co., China. All solutions were prepared with deionized water. RhB stock solution (500 mg·$L^{-1}$) was prepared in deionized water, and stored at 4 °C in the dark. The reaction solutions were freshly prepared by diluting the stock solution with deionized water. The initial pH of the reaction solution was adjusted by either 0.1 M HCl or 0.1 M NaOH when necessary. The titanium mesh with 1 mm thickness (>99.6% purity) was purchased from Shengyuan Co. Ltd., China, and was processed into the specification of 5 cm × 5 cm with a tail for electrochemical test.

**2.2. Fabrication of the Sb-Doped $SnO_2$/Ti Electrode.** The preparation of the Sb-doped $SnO_2$/Ti electrode using a triethanolamine-assisted method has been described in our previous work.[33] Briefly, the titanium mesh was burnished with sandpaper (120 mesh), cleaned with ultrapure water, and then sonicated in 1.0 M NaOH solution for 30 min to remove organic-like substances and oxides. Second, the treated Ti-mesh was soaked in 10% oxalic acid solution at 80 °C until the convex-concave structure appeared on the plate surface and then stored in methanol for oxidation resistance. $Sb_2O_3$ (6.0 g) was first dissolved in 25 mL of 0.3 M HCl to form $SbCl_3$ solution, and then 300 mL of triethanolamine (TEA) was added and stirred at room temperature (25 ± 2 °C). Subsequently, 600.0 g of $SnCl_2{\cdot}2H_2O$ was mixed with the above solution and stirred for 3 h to obtain a white viscous solution. Finally, the viscous solution was mixed with 62.0 mL of a 34% $Na_2SiO_3$ solution and 10.0 mL of a 1.0 M NaOH solution to form the precursor. To fabricate the Sb-doped $SnO_2$/Ti electrode, the precursor was sprayed uniformly onto the Ti mesh and immediately transferred into a furnace. The coated Ti-mesh was calcined at 450 °C for 10 min, and then cooled to the room temperature. The aforementioned treatments were repeated for three times, and the last calcination process was performed for 1 h.

**2.3. Characterization of the Sb-Doped $SnO_2$/Ti Electrode.** The surface morphology, elemental composition, phase analysis, and structure of the Sb-doped $SnO_2$/Ti electrode before and after use were characterized by scanning electron microscopy (SEM, Zeiss supra55, Germany), energy dispersive spectrometry (EDS, Oxford X-max 80, Britain), X-ray diffraction (XRD, Bruker D8 Advance, Germany) and X-ray photoelectron spectroscopy (XPS, Thermo Scientific ESCALAB 250Xi, USA), respectively.

The electrochemical performance of the Sb-doped $SnO_2$/Ti electrode was assessed by a three-electrode cell system connected to an electrochemical workstation (CHI660E, Chenhua Co., Ltd., China). The Sb-doped $SnO_2$/Ti electrode, Ti-mesh (5 cm × 5 cm), and Hg/HgO electrode were used as the working electrode, auxiliary electrode, and reference electrode, respectively. During the test, 10 mg·$L^{-1}$ RhB solution (pH 11) was employed for cyclic voltammetry (CV) analysis with a sweep rate of 50 mV·$s^{-1}$ and a scan range from


https://doi.org/10.1021/acsomega.3c08391
ACS Omega 2023, 8, 48480−48490

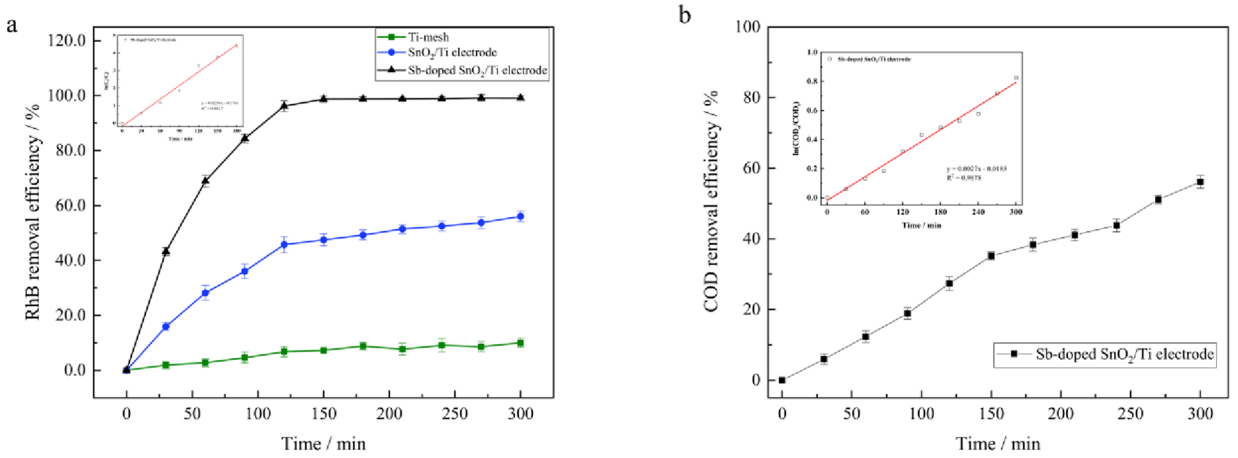


**Figure 1.** Variations of RhB removal efficiency (a) and COD removal efficiency (b) during the electrochemical oxidation (the inserts indicate the degradation kinetic curves of RhB and COD by using the Sb-doped $SnO_2$/Ti electrode) (the initial concentration of RhB: 50 mg·$L^{-1}$, the initial pH of the reaction solution: 11).

−1.50 to 1.50 V. The stability of the Sb-doped $SnO_2$/Ti electrode was investigated by the current−time ($i$−$t$) mode. The $i$−$t$ curve was obtained in a NaOH solution (pH 11) for 14 h at an applied voltage of 10.0 V.

**2.4. Performance for the Degradation of RhB.** The schematic diagram of the electrochemical degradation device is shown in Figure S1 (Supporting Information). Five hundred milliliters of RhB solution (pH 11) was added into a 600 mL electrolytic cell, and then the Sb-doped $SnO_2$/Ti electrode (5.0 cm × 5.0 cm) and Ti-mesh (5.0 cm × 5.0 cm) were inserted into the electrolytic cell with a distance of 1 cm and served as the anode and the cathode, respectively. The electrochemical degradation of RhB was carried out at a constant voltage of 5.0 V at room temperature. The reaction solution (1 mL) was collected at a certain time interval for RhB detection, and the removal efficiency was calculated according to the concentration change of RhB.

**2.5. Degradation of Real Dye Wastewater.** The indigo production wastewater was collected from Huacai Chemical Industrial Co., Ltd. (Chongqing, China) and was used as real dye wastewater for the electrochemical degradation by an Sb-doped $SnO_2$/Ti electrode. The indigo production wastewater had been pretreated by the sewage treatment station in the factory, and its color was yellow-brown. The pH of this wastewater was 10, and the COD concentration was about 700 mg·$L^{-1}$. The pH and COD concentration of this wastewater are both higher than the values (pH 6−9, COD 80 mg·$L^{-1}$) set in the discharge standards of water pollutants for dyeing and finishing of the textile industry of China (GB 4287−2012). Five hundred milliliters of dye wastewater sample was added into the electrolytic cell, and then the electrochemical degradation was carried out according to Section 2.4.

**2.6. Sample Analytical Methods.** The concentration of RhB was measured by a UV−vis absorption spectrometer (UV1800, Persee, China) at 555 nm. The chemical oxygen demand of the reaction solution was determined with a COD measurement apparatus (ET99722 Lovibond, Germany). The degradation products of RhB were identified by a liquid chromatography−mass spectrometry instrument (LC-MS, LC-2020, Shimadazu, Japan) with ShimNex HE $C_{18}$ column (250 mm × 4.6 mm, 5 $\mu$m, Shimadazu, Japan). Mobile phases A and B were acetonitrile and 0.1% formic acid, respectively. The gradient elution program was used as follows: 0 → 10 min, mobile phase A 5%; 10 → 30 min, A 5% → 60%; 30 → 45 min, A 60% → 95%; 45 → 50 min, A 95% → 5%. The separation was carried out at the column temperature of 40 °C with a flow rate of 1 mL·$min^{-1}$, and the injection volume was 10 $\mu$L. The MS spectra were monitored by full scan mode and operated by using an electrospray ion source in negative and positive ion modes. The capillary voltage was 4.5 kV, and high-purity nitrogen was used as the collision gas, cone gas, and atomizing gas.

The concentration of hydroxyl radical was calculated according to the product (2,5-dihydroxybenzoic acid) amount by using salicylic acid (SA) as a probe. 2,5-Dihydroxybenzoic acid (2,5-DHBA) was determined by high-performance liquid chromatography (HPLC, LC-20A, Shimadazu, Japan) with an Inertsil ODS-SP column (250 × 4.6 mm, 5 $\mu$m, Shimadazu GL-science, Japan) at 30 °C. Mobile phases consisted of methanol and 0.05% phosphoric acid (40:60, V/V) with a flow rate of 1 mL·$min^{-1}$, isocratic elution. The injection sample volume was 20 $\mu$L, and the UV detection wavelength was 320 nm.

## 3. RESULTS AND DISCUSSION

**3.1. Electrocatalytic Degradation Performance of RhB in Alkaline Medium.** To investigate the electrocatalytic degradation performance of RhB in an alkaline medium, 50 mg·$L^{-1}$ RhB was degraded in the simulated alkaline wastewater, and the obtained results are shown in Figure 1a. It can be found that the removal efficiency of RhB can reach 68.9% in 60 min and achieve nearly 100% in 150 min with the Sb-doped $SnO_2$/Ti electrode, while they are only 56.1% and 10.0% in 300 min with the nondoped $SnO_2$/Ti electrode and Ti-mesh electrode, respectively. These results demonstrate that Sb doping in the active layer can significantly improve the electrocatalytic activity of the $SnO_2$/Ti electrode. In order to provide a more comprehensive description of the electrocatalytic process of RhB, COD removal was used as the evaluation index to investigate the mineralization effect (Figure 1b). Different from the significant increase in RhB removal observed in the first 60 min, the COD removal shows a relatively gentle declining trend and reaches 56.1% after 300 min. The reason may be that the intermediate products compete with RhB for hydroxyl radicals, ultimately reducing the mineralization efficiency of RhB.


https://doi.org/10.1021/acsomega.3c08391
ACS Omega 2023, 8, 48480−48490

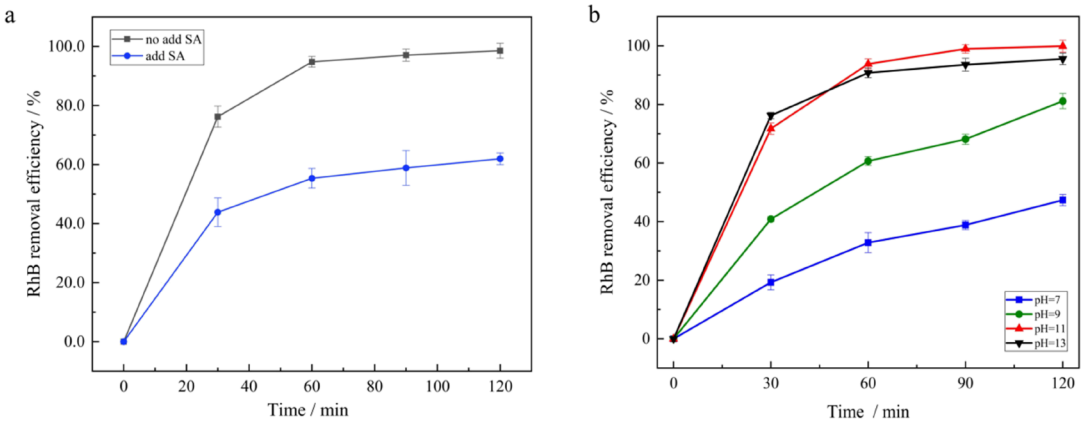


**Figure 2.** Effect of salicylic acid (a) and the initial pH (b) on RhB degradation (the initial concentrations of RhB and SA: 25 mg·$L^{-1}$).

Using the Sb-doped $SnO_2$/Ti electrode, the removal processes of RhB and COD followed the pseudo-first-order reaction kinetic equation, and the kinetic curves are shown in the insets of Figure 1a,b. The results indicate that the degradation processes of RhB follow this model very well ($R^2$ > 0.98), implying that diffusion played a dominant role during the degradation process.[34] The removal rate constants of RhB and COD can be calculated as 0.0258 and 0.0027 $min^{-1}$, respectively. Compared with other electrodes (Table S1, Supporting Informations), the removal efficiencies and rate constants of RhB by Sb-doped $SnO_2$/Ti electrode are higher than those by $PbO_2$ electrodes,[19,20] $NiCo_2O_4$ electrode[25] and particle electrode,[27] but lower than those with BDD electrode,[15] $TiO_2$ nanoclusters/Sb-$SnO_2$ electrode,[22] porous Au electrode,[26] and CNTs/AG membrane on ITO electrode.[28] In this work, we degraded RhB in alkaline medium; however, other studies degraded RhB usually in a neutral or acidic medium, and the removal efficiency of RhB in alkaline medium involved in these studies is lower than that of our work. Considering the electrode materials, electrode preparation, and degradation performance, the Sb-doped $SnO_2$/Ti electrode has good application potential in the treatment of alkaline dye wastewater.

**3.2. Role of Hydroxyl Radicals in the Electrocatalytic Degradation of RhB.** Electrocatalytic degradation of organic compounds can be accomplished through both direct and indirect oxidation. Direct oxidation refers to the fact that organic molecules are adsorbed on the electrode surface and then directly oxidized with a low reaction rate, not involving anything other than electrons. In indirect oxidation, organic molecules are oxidized by electro-generated reactive species (e.g., ·OH, $S_2O_8^{2-}$, $ClO^-$ and $O_2^{\cdot-}$), which does not require the addition of oxidant and can increase the mineralization efficiency of the organic pollutant.[35] In addition to ·OH, the formation of other reactive species was related to the nature of the supporting electrolyte.[34] In this work, no supporting electrolyte was used and no other reactive species were generated in the reaction system except ·OH, so the oxidation of RhB caused by other reactive species can be neglected. Based on the strong ability of salicylic acid (SA) to capture ·OH and the stability of its hydroxylation product (2,5-DHBA),[36] 25 mg·$L^{-1}$ SA was used as the scavenger to evaluate the role of ·OH in RhB degradation, and the obtained results are shown in Figure 2a. It can be found that the removal efficiencies of 25 mg·$L^{-1}$ RhB are 76.2, 94.8, 97.1, and 98.6% at 30, 60, 90, and 120 min in the absence of SA, whereas those are 43.8, 55.3, 58.9, and 62.0% in the presence of SA, respectively. These results indicate that partial ·OH radicals are captured by SA, which can obviously inhibit the degradation of RhB, suggesting that ·OH plays the main role in the electrocatalytic degradation of RhB.

The amount of reactive species generated in the electrochemical process can be controlled by many factors, including the treatment technique, electrode, the pH of the reaction solution, etc.[34] The variations of RhB removal in different pH solutions can indirectly reflect the electrocatalytic oxidation of RhB by ·OH radicals in this system. As shown in Figure 2b, the removal efficiencies of RhB are 47.4, 81.2, 99.9, and 95.6% at the initial pH of 7, 9, 11, and 13 at 120 min, respectively. It should be noted that the maximum removal efficiency is obtained in a pH 11 solution at 90 min. Under alkaline conditions, the electrode surface becomes negatively charged, which induces a significant number of hydroxyl ions to be adsorbed on the tight layer of the double electric layer.[37] During the electrocatalytic degradation of RhB, hydroxyl ions are oxidized by the reactive oxygen species within the metal lattice and cause the transfer of outer layer electrons, thereby promoting the generation of hydroxyl radicals and enhancing RhB degradation.

As an active free radical, ·OH can not only have strong oxidation ability in the electrolytic process but also oxidize organic molecules into $CO_2$ and $H_2O$. Therefore, as the ·OH scavenger, excess SA was added separately to the electrocatalytic oxidation system to assess the ·OH generation capability of the Sb-doped $SnO_2$/Ti electrode, and the ·OH concentration can be calculated through 2,5-DHBA concentration based on the stoichiometric relationship between SA and ·OH. As the time increases, the amount of 2,5-DHBA gradually increases (Figure S2, Supporting Information), demonstrating that ·OH radicals are generated gradually with the increase of reaction time. The generation rate of ·OH can be represented by the slope of the linear fitting curve of the ·OH concentration versus the reaction time, which was 0.3776 mol·$L^{-1}$·$min^{-1}$.

**3.3. Morphological and Structural Changes of the Sb-Doped $SnO_2$/Ti Electrode before and after Use.** The surface morphology of the Sb-doped $SnO_2$/Ti electrode before and after use was characterized by SEM, and it is shown in Figure 3. It can be seen that the surface of the Sb-doped $SnO_2$/Ti electrode before use is compact and exhibits a flat and lamellar morphology, and the coatings of the partial area display a multilayer structure and cluster structure (Figure 3a),


https://doi.org/10.1021/acsomega.3c08391
ACS Omega 2023, 8, 48480−48490

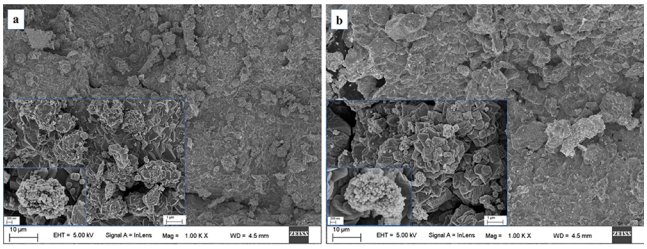

**Figure 3.** SEM images of Sb-$SnO_2$/Ti before (a) and after use (b).

likely due to the multiple spraying and pyrolysis. After the electrochemical degradation in alkaline medium for 7 h, the used electrode shows a similar surface morphology to the freshly prepared one with no obvious "crack-mud" structure (Figure 3b), indicating that the coatings have good adhesive properties to the Ti substrate, and the relatively intact and dense oxide coatings possibly improve the corrosion resistance of the electrode, thus prolonging its service life.[38]

The XRD patterns of the Sb-doped $SnO_2$/Ti electrode and the Ti mesh are shown in Figure 4a. Apparently, no diffraction peaks corresponding to titanium are observed in the XRD pattern of the Sb-doped $SnO_2$/Ti electrode, which proves that the active coatings uniformly and densely cover the Ti substrate, and can effectively prevent the formation of the $TiO_2$ passivation layer during the electrocatalytic process.[39] The results of the EDS analysis (Figure S3, Supporting Information) also confirm this conclusion. A series of diffraction peaks of the Sb-doped $SnO_2$/Ti electrode are observed at 26.60°, 33.84°, 37.95°, 51.74°, 54.73°, 61.85°, 64.68°, 65.93°, and 78.60° ($2\theta$), assigned to the (110), (101), (200), (211), (220), (310), (112), (301), and (321) crystal planes of $SnO_2$, respectively.[40] These peaks are consistent with the standard data in PDF card No. 41-1445 of $SnO_2$, demonstrating that the surface coatings on Ti mesh are primarily composed of $SnO_2$ crystals with a tetragonal structure.[41] Particularly, the diffraction peaks at 26.60°, 33.84°, and 51.74° are sharp and strong, indicating that $SnO_2$ is polycrystalline with three dominant crystal planes.[42] No diffraction peaks corresponding to Sb and its oxide are observed in the XRD pattern of the Sb-doped $SnO_2$/Ti electrode, but the EDS results proved the presence of Sb (Figure S3, Supporting Information), indicating that the surface coating is primarily composed of $SnO_2$ crystal, while Sb does not form a separate phase. Due to a similar ionic radius with $Sb^{5+}$ (0.61 Å) and $Sn^{4+}$ (0.71 Å), $Sb^{5+}$ could enter into the crystal lattice of $SnO_2$ as an ion form to replace $Sn^{4+}$ at high temperatures.[43] Compared with the freshly prepared electrode, the main peaks and their intensities are nearly identical, and no additional diffraction peaks are detected in the XRD pattern of the used electrode, indicating that the crystal structure of $SnO_2$ remains unchanged after use and the Sb-doped $SnO_2$/Ti electrode exhibits good stability.

The chemical composition and oxidation state of each element on the electrode surface were examined by XPS (Figure 4b). The results confirm the existence of Sn, Sb, N, C, and Cl in the Sb-doped $SnO_2$/Ti electrode before and after use. The small amount of Cl detected on the electrode surface likely originates from $SbCl_3$ and $SnCl_2{\cdot}2H_2O$, and the presence of C and N elements may be mainly attributed to the addition of triethanolamine during the electrode preparation process. A comparison of the Sn 3d spectra of the electrode before and after use is shown in Figure 4c. The two strong and asymmetric peaks of Sn 3d correspond to the binding energy positions of 486.9 and 495.3 eV, with a gap of approximately 8.4 eV between them, which are consistent with the reported data of spin−orbit splitting, demonstrating that Sn is in +4 valence state and exists in the form of $SnO_2$.[33,44] The Sn 3d binding energy of the freshly prepared electrode is slightly higher than that of the electrode after use, which may be attributed to the different bonding environments of Sn atom at the interface of $SnO_2$, indicating that the average electron density around $Sn^{4+}$ in the freshly prepared electrode is lower than that of the electrode after use.[45] The XPS spectra of Sb $3d_{5/2}$ and O 1s are overlapped, showing the mixed spectra after the peak splitting treatment of the electrode before and after use in Figure 4d,e. The binding energy position at ∼530.8 eV corresponds to the characteristic peak of Sb $3d_{5/2}$, demonstrating the presence of $Sb^{5+}$, which can provide plenty of free electrons to narrow the band gap of $SnO_2$ and improve its conductivity, leading to more hydroxyl radicals physically adsorbed.[46−48] The O 1s peak consists of two peaks with binding energy values at ∼530.4 and ∼531.7 eV, respectively. The former is attributed to the lattice oxygen $O_{lat}$ originated from the metal oxide ($SnO_2$), while the latter is referred to as the adsorbed oxygen ($O_{ads}$) associated with the adsorbed hydroxyl oxygen species (Sn−OHs) and/or hydrated species.[49−51] $O_{ads}$ can participate in the generation of reactive oxygen species at the electrode−solution interface, and play an important role in the electrocatalytic oxidation process.[52] Figure 4d,e show that the percentages of $O_{ads}$ and $O_{lat}$ on the electrode surface have changed obviously before and after use. The intensity change of the $O_{lat}$ peak exhibits an increasing trend, while the intensity of the $O_{ads}$ peak decreases after the electrode use, which may be due to the participation of the adsorbed hydroxyl in the electrocatalytic oxidation of RhB.[14]

**3.4. Electrochemical Performance Change of the Sb-Doped $SnO_2$/Ti Electrode.** Figure 4f shows the CV curves of the Sb-$SnO_2$/Ti electrode in 10 mg·$L^{-1}$ RhB solution (pH 11). The current density initially decreases and then partially recovers with the increase of scanning times, suggesting that the freshly prepared electrode shows much better electrocatalytic oxidation activity and then slightly decreases with the continuous run. This is likely due to the interaction between the surface-adsorbed hydroxyl groups and the unstable Sn atoms formed by the dissolution of $SnO_2$ lattice under alkaline conditions, resulting in the formation of the nonconducting Sn−OH, which can impair the electrochemical activity of the electrode to some extent. However, the generation of hydroxyl radicals during the electrolytic process causes the transformation of Sn−OHs into $SnO_2$, thereby reinforcing the activity and stability of the electrode.[53] The high oxygen evolution potential (OEP) of the electrode is critical for the generation of hydroxyl radical, which can facilitate free radical production and reduce the current loss due to the oxygen evolution reaction during electrochemical oxidation. Correspondingly, changes in the OEP during electro-oxidation were also observed. In the beginning, the OEP of electro-oxidation of RhB is around 1.52 V (vs RHE) but shifts to 1.66 V (vs. RHE) after scanning 500 cycles. The increase of OEP demonstrates that the Sb-doped $SnO_2$/Ti electrode prefers to generate $^{\cdot}OH$ for the oxidation of RhB rather than converting into $O_2$ at the same potential, and thus the electrocatalytic activity of the electrode is partially restored.[54] After scanning 500 cycles, the appearances of the oxidation peaks at −0.02 and 1.40 V, and the reduction peaks at −0.14


https://doi.org/10.1021/acsomega.3c08391
ACS Omega 2023, 8, 48480−48490

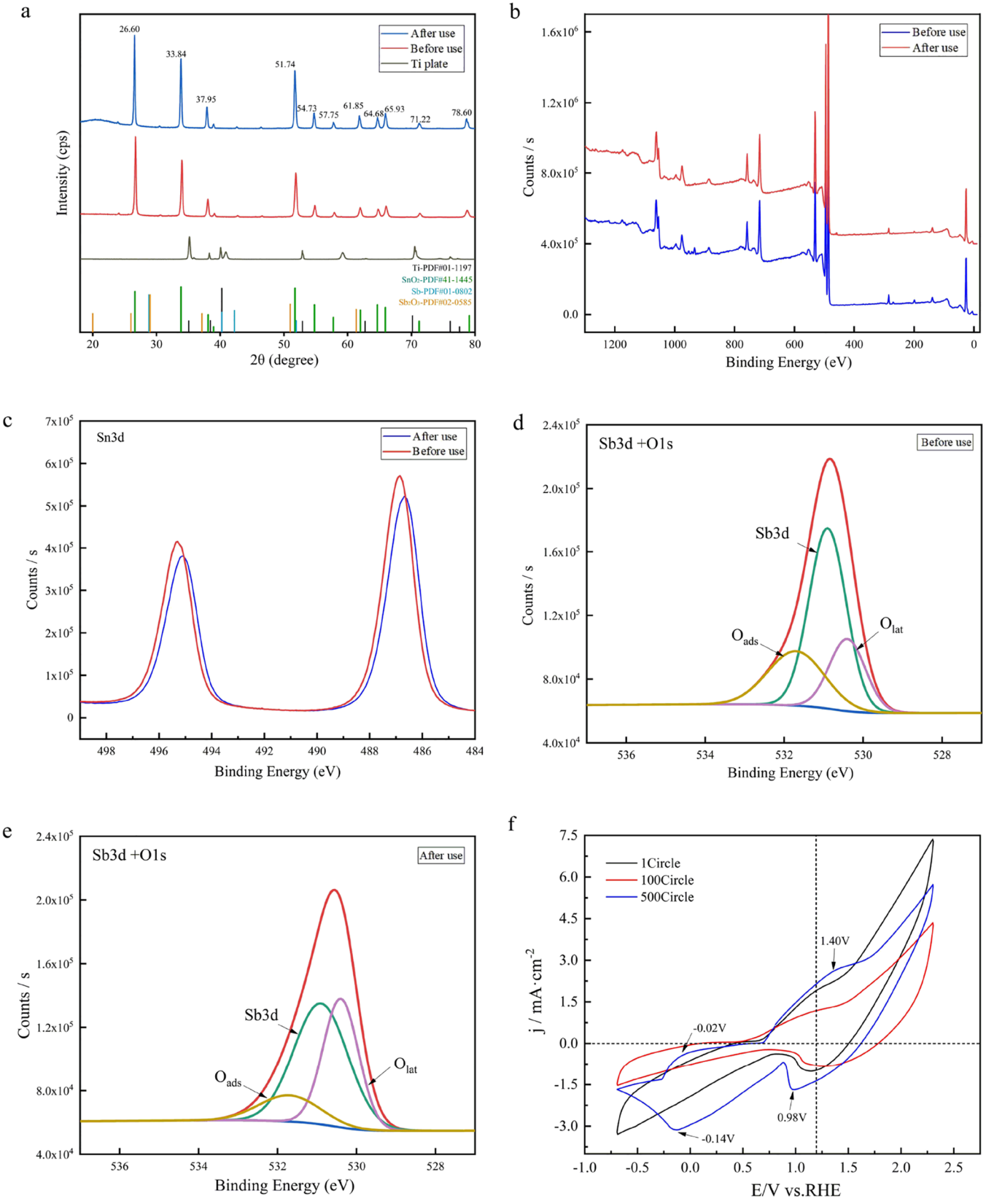


**Figure 4.** XRD patterns (a), XPS spectra (b), high-resolution XPS spectra of Sn 3d (c), high-resolution XPS spectra of O 1s and Sb 3d (d and e) of the Sb-doped $SnO_2$/Ti electrode before and after use, and CV curves (f) of the Sb-$SnO_2$/Ti electrode in RhB solution (pH 11).

and 0.98 V on the blue curve indicate that the valence state of Sn or Sb on the electrode surface has changed, which can promote the production of ·OH.[55]

**3.5. Degradation Mechanism of RhB by the Sb-Doped $SnO_2$/Ti Electrode.** The UV−vis absorption spectra and discoloration effects during RhB degradation were



https://doi.org/10.1021/acsomega.3c08391
ACS Omega 2023, 8, 48480−48490

detected, and the results are shown in Figure 5a,b, respectively. Because the absorption of RhB is mainly due to the large

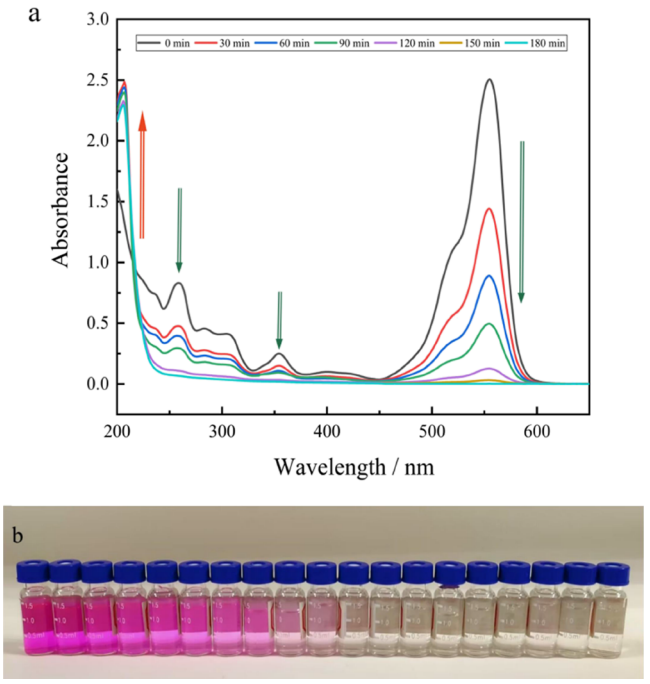


**Figure 5.** UV−vis spectra (a) and discoloration effects (b) of RhB solution during the electrochemical oxidation (the initial concentration of RhB: 50 mg·$L^{-1}$, and the initial pH of the reaction solution: 11).

conjugated chromophore, the characteristic absorption peak intensities of RhB at 261, 354, and 555 nm gradually decrease with the degradation of RhB, indicating that large conjugated chromophores are attacked by hydroxyl radicals. The predominant absorption peak at 555 nm determines the chroma of RhB, and the weakening of the peak intensity at 555 nm leads to the decolorization of the sample solution. Moreover, the weakening of the absorption peak intensity at 354 nm indicates that the accumulation of highly toxic quinone compounds is not observed.[33] It is noteworthy that a new strong absorption peak appears around 207 nm at 30 min, which is attributed to the formation of more aromatic compounds during RhB degradation. Combining the removal results of RhB and COD, we speculate that the skeleton structure of xanthene and some functional groups, such as multiple conjugated chromophores by carbon−carbon double bonds, are destroyed during RhB degradation.

The degradation intermediate products of RhB were identified by HPLC-MS, and the obtained results are presented in Table S2 (Supporting Information), and the possible degradation pathways of RhB are proposed in Figure 6. The first step of RhB degradation is the N-de-ethylation. The p-type electron orbital of N is bound to the benzene ring, making the ethyl group at the N-position easily attacked due to electron delocalization. Therefore, hydroxyl radicals produced in the electrocatalytic oxidation first cause the N-de-ethylation of RhB to form product I ($C_{26}H_{27}N_2O_3^+$, $m/z$ = 415), product II ($C_{24}H_{23}N_2O_3^+$, $m/z$ = 387), product III ($C_{20}H_{15}N_2O_3^+$, $m/z$ = 331).[14,56] Subsequently, hydroxyl radicals attack the N-de-ethylation products to induce denitrification and decarboxylation reactions, thus forming product IV ($C_{20}H_{15}NO_3$, $m/z$ = 318) and product V ($C_{19}H_{15}NO$, $m/z$ = 274).[57] Then, hydroxyl radicals continue to attack the structural center of RhB, leading to the destruction of the conjugated xanthene structure, e.g., the cleavage and ring-opening of product V form product VI ($C_{13}H_9O$, $m/z$ = 181) and small molecule organic

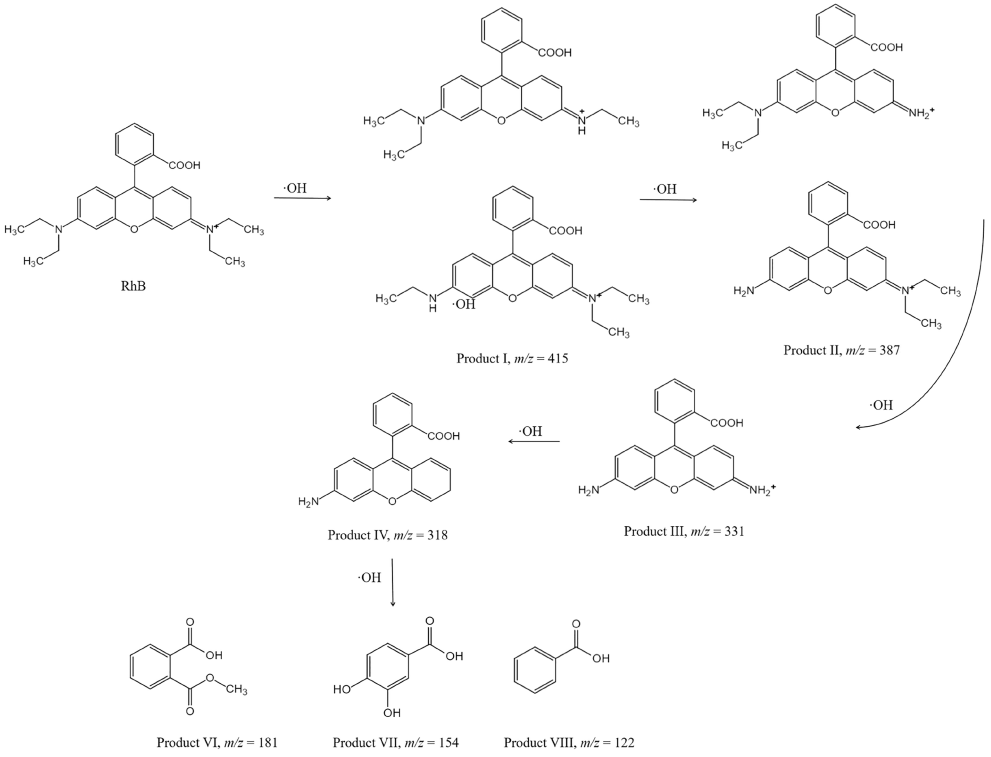


**Figure 6.** Possible Electrochemical Degradation Pathways of RhB.



https://doi.org/10.1021/acsomega.3c08391
ACS Omega 2023, 8, 48480−48490

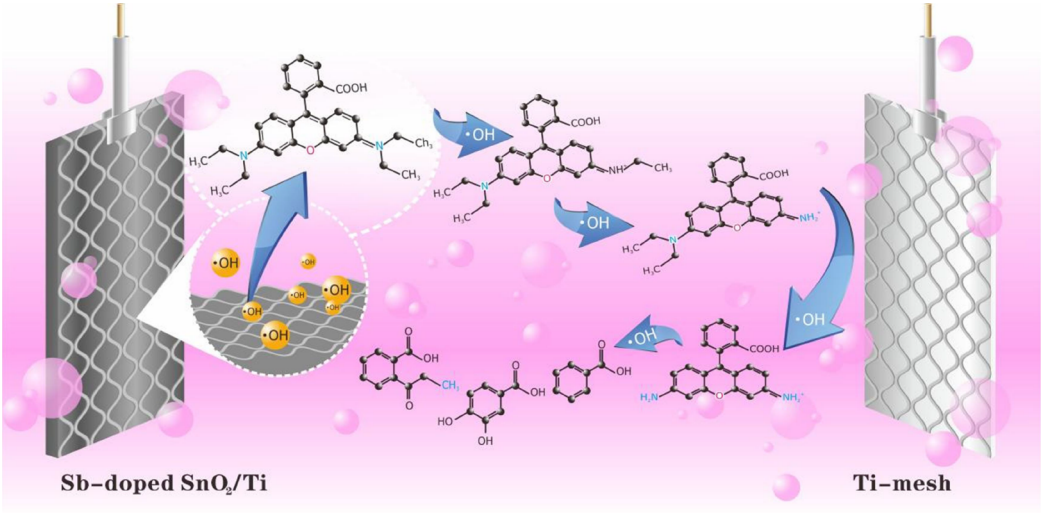


**Figure 7.** Schematic illustration of the electrocatalytic oxidation mechanism of RhB.

acids, such as product VII ($C_7H_6O_4$, $m/z$ = 154) and product VIII ($C_7H_6O_2$, $m/z$ = 122).[56]

Combining the analysis of the degradation pathways and UV−vis absorption spectra, the degradation mechanism of RhB using the Sb-doped $SnO_2$/Ti electrode was speculated, and the schematic illustration is shown in Figure 7. During the electrocatalytic oxidation of RhB, a great number of ·OH radicals are generated on the surface of the Sb doped-$SnO_2$/Ti electrode. ·OH radicals can attack RhB and its oxidation products, causing the N-de-ethylation of RhB and cleavage of chromophore groups, and then, the cleavage products of chromophore groups can be oxidized to low-molecular-weight organic acids through ring opening and eventually be converted into $CO_2$ and $H_2O$ through further mineralization.

**3.6. Characteristics of the Sb-Doped $SnO_2$/Ti Electrode.** The reproducibility, reusability, and stability of the Sb-doped $SnO_2$/Ti electrode deserve careful attention for the real applications. A low RSD of removal efficiency (3.8% for 50 mg·$L^{-1}$ RhB) was obtained by three electrodes prepared in one batch. Batch-to-batch reproducibility was investigated by the electrodes prepared in six batches, among which the RSD of removal efficiency was 5.2% for 50 mg·$L^{-1}$ RhB, further implying that the Sb-doped $SnO_2$/Ti electrode can be prepared repeatedly. The reusability was investigated by repeating RhB degradation for eight cycles using the same electrode, and the results are shown in Figure S4a (Supporting Information). It can be observed that the removal efficiency of RhB exhibits a slight decline with the increase of cycle number of the electrode and is still up to 93.2% after eight cycles, which maintains 94.1% of the initial removal efficiency. Furthermore, the $i$−$t$ curve of the Sb-doped $SnO_2$/Ti electrode was tested under an applied voltage of 10.0 V in NaOH solution (Figure S4b, Supporting Information). It can be seen that the current remains at ∼250 mA, even though the electrochemical reaction lasts for 840 min, showing that the electrolytic performance of the electrode does not change significantly. Combined with the results of the repeating experiments and $i$−$t$ curve, the Sb-doped $SnO_2$/Ti electrode has high stability.

In order to evaluate the safety of the reaction solution after electrolysis, Sb concentrations in the degradation system were measured at 4 and 24 h by ICP-MS. No Sb ion was detected at 4 h degradation, while the dissolved Sb (0.004 mg·$L^{-1}$) was detected at 24 h degradation, which is significantly lower than the discharge standards of water pollutants for dyeing and finishing of textile industry of China (<0.1 mg·$L^{-1}$, GB 4287-2012) and emission standards of pollutants for stannum, antimony and mercury industries of China (<0.3 mg·$L^{-1}$, GB 30770-2014). These results indicated that the Sb-doped $SnO_2$/Ti electrode has good reusability, high stability, and low antimony-leaching risk and meets the requirements of RhB degradation.

**3.7. Application to the Treatment of Real Dye Wastewater.** In order to assess the practicability of the proposed method, an indigo wastewater sample (pH 10, COD ∼ 700 mg·$L^{-1}$) was degraded by the Sb-doped $SnO_2$/Ti electrode, and the obtained results are shown in Figure S5 (Supporting Information). It can be observed that the wastewater becomes colorless after 12 h degradation, and the removal efficiency of COD reaches 90.1% with its concentration below the discharge standard value of China (<80 mg·$L^{-1}$, GB 4287-2012). After 24 h degradation, the COD concentration is below the detection limit (<4 mg·$L^{-1}$), indicating that most of organic compounds in this wastewater have been converted into $CO_2$ and $H_2O$. Therefore, the Sb-doped $SnO_2$/Ti electrode is a promising anode to efficiently remove of dye in real wastewater.

## 4. CONCLUSIONS

In this work, an Sb-doped $SnO_2$/Ti electrode was used to degrade RhB in an alkaline medium. The removal efficiency of 50 mg·$L^{-1}$ RhB in alkaline solution (pH 11) reached 99.1% after 150 min of degradation, and the degradation process followed the first-order reaction kinetic model very well. This electrode displayed high stability in alkaline medium based on the morphological and structural changes and $i$−$t$ curves before and after use. Hydroxyl radicals (·OH) played a very important role in RhB degradation, which could destroy the stable chemical structure of RhB and realize effective mineralization. The electrode showed high reusability, stability, and safety during the degradation of RhB in alkaline medium, and has been successfully applied to the treatment of real dye wastewater. Electrocatalytic degradation is a promising technology to treat alkaline dye wastewater by the Sb-doped $SnO_2$/Ti electrode.



https://doi.org/10.1021/acsomega.3c08391
ACS Omega 2023, 8, 48480−48490

## ■ ASSOCIATED CONTENT

### Supporting Information

The Supporting Information is available free of charge at https://pubs.acs.org/doi/10.1021/acsomega.3c08391.

Experimental details; device schematic diagram; EDS image of the electrode surface; ·OH generation capability; stability and practicability tests; RhB degradation intermediate products; and comparison of previously reported electrodes for electrochemical degradation of RhB (PDF)

## ■ AUTHOR INFORMATION


### Corresponding Author

**Ying Li** − *Chemical Pollution Control Chongqing Applied Technology Extension Center of Higher Vocational Colleges, Chongqing Industry Polytechnic College, Chongqing 401120, P.R. China;* orcid.org/0000-0002-7043-9962; Phone: +86-23-61879011; Email: yingli@cqipc.edu.cn; Fax: +86-23-61879228

### Authors

**Dongli Deng** − *Chemical Pollution Control Chongqing Applied Technology Extension Center of Higher Vocational Colleges, Chongqing Industry Polytechnic College, Chongqing 401120, P.R. China;* orcid.org/0009-0004-8248-9758

**Mingzhu Wu** − *Chemical Pollution Control Chongqing Applied Technology Extension Center of Higher Vocational Colleges, Chongqing Industry Polytechnic College, Chongqing 401120, P.R. China*

**Yang Song** − *Chemical Pollution Control Chongqing Applied Technology Extension Center of Higher Vocational Colleges, Chongqing Industry Polytechnic College, Chongqing 401120, P.R. China*

**Qiongjian Huang** − *Chemical Pollution Control Chongqing Applied Technology Extension Center of Higher Vocational Colleges, Chongqing Industry Polytechnic College, Chongqing 401120, P.R. China*

**Yiqin Duan** − *Chemical Pollution Control Chongqing Applied Technology Extension Center of Higher Vocational Colleges, Chongqing Industry Polytechnic College, Chongqing 401120, P.R. China*

**Yu Chang** − *Chemical Pollution Control Chongqing Applied Technology Extension Center of Higher Vocational Colleges, Chongqing Industry Polytechnic College, Chongqing 401120, P.R. China*

**Yangyang Zhao** − *Chemical Pollution Control Chongqing Applied Technology Extension Center of Higher Vocational Colleges, Chongqing Industry Polytechnic College, Chongqing 401120, P.R. China*

**Chunling He** − *Chemical Pollution Control Chongqing Applied Technology Extension Center of Higher Vocational Colleges, Chongqing Industry Polytechnic College, Chongqing 401120, P.R. China*

Complete contact information is available at: https://pubs.acs.org/10.1021/acsomega.3c08391


### Notes

The authors declare no competing financial interest.

## ■ ACKNOWLEDGMENTS

This work was supported by Chongqing Postdoctoral Science Fund (No. CSTB2023NSCQ-BHX0035), Science and Technology Research Programs of Chongqing Education Commission of China (No. KJZD-K202203204, KJZD-K202303201), Science and Technology Plan Project of Chongqing Yubei District Science and Technology Bureau (No. YBKJNS202202).

## ■ REFERENCES


(1) Katheresan, V.; Kansedo, J.; Lau, S. Y. Efficiency of various recent wastewater dye removal methods: A review. *J. Environ. Chem. Eng.* **2018**, *6*, 4676−4697.

(2) Velusamy, S.; Roy, A.; Sundaram, S.; Mallick, T. K. A review on heavy metal ions and containing dyes removal through graphene oxide-based adsorption strategies for textile wastewater treatment. *Chem. Rec.* **2021**, *21*, 1570−1610.

(3) Huang, Z.; Bu, J.; Wang, H. Adsorption effect of two modified kaolin materials on wastewater containing multi-component organic dyes. *Desalin. Water Treat.* **2022**, *250*, 266−287.

(4) Prajapati, K.; Sorokhaibam, L. G.; Bhandari, V. M.; Killedar, D. J.; Ranade, V. V. Differentiating process performance of various coagulants in removal of Congo red and Orange G dyes. *Int. J. Chem. React. Eng.* **2016**, *14*, 195−211.

(5) Jia, J.; Wu, H.; Xu, L.; Dong, F.; Jia, Y.; Liu, X. Removal of acidic organic ionic dyes from water by electrospinning a polyacrylonitrile composite MIL101(Fe)-$NH_2$ nanofiber membrane. *Molecules* **2022**, *27*, 2035.

(6) Gui, L.; Peng, J.; Li, P.; Peng, R.; Yu, P.; Luo, Y. Electrochemical degradation of dye on $TiO_2$ nanotube array constructed anode. *Chemosphere* **2019**, *235*, 1189−1196.

(7) Vinothkannan, M.; Karthikeyan, C.; Gnana Kumar, G.; Kim, A. R.; Yoo, D. J. One-pot green synthesis of reduced graphene oxide (RGO)/$Fe_3O_4$ nanocomposites and its catalytic activity toward methylene blue dye degradation. *Spectrochim. Acta, Part A* **2015**, *136*, 256−264.

(8) Jenita Rani, G.; Jothi Rajan, M. A.; Gnana Kumar, G. Reduced graphene oxide/$ZnFe_2O_4$ nanocomposite as an efficient catalyst for the photocatalytic degradation of methylene blue dye. *Res. Chem. Intermed.* **2017**, *43*, 2669−2690.

(9) Brillas, E.; Martinez-Huitle, C. A. Decontamination of wastewaters containing synthetic organic dyes by electrochemical methods. An updated review. *Appl. Catal. B: Environ.* **2015**, *166−167*, 603−643.

(10) Sun, W. H.; Liu, D. F.; Zhang, M. H. Application of electrode materials and catalysts in electrocatalytic treatment of dye wastewater. *Front. Chem. Sci. Eng.* **2021**, *15*, 1427−1443.

(11) Yusuf, T. L.; Orimolade, B. O.; Masekela, D.; Mamba, B.; Mabuba, N. The application of photoelectrocatalysis in the degradation of rhodamine B in aqueous solutions: A review. *RSC Adv.* **2022**, *12*, 26176−26191.

(12) Shi, X.; Hong, P.; Huang, H.; Yang, D.; Zhang, K.; He, J.; Li, Y.; Wu, Z.; Xie, C.; Liu, J.; Kong, L. Enhanced peroxymonosulfate activation by hierarchical porous $Fe_3O_4/Co_3S_4$ nanosheets for efficient elimination of rhodamine B: Mechanisms, degradation pathways and toxicological analysis. *J. Colloid Interface Sci.* **2022**, *610*, 751−765.

(13) Li, K. H.; Xiao, Y.; Zhao, Y. C.; Xia, Y. H.; Ding, J. H.; He, Q. G.; Ling, J.; Li, G. L. A metal-free voltammetric sensor for sensitive determination of Rhodamine B using carboxyl-functionalized carbon nanomaterials. *Inorg. Chem. Commun.* **2022**, *145*, No. 110025.

(14) He, Q. G.; Liu, J.; Xia, Y. H.; Tuo, D.; Deng, P. H.; Tian, Y. L.; Wu, Y. Y.; Li, G. L.; Chen, D. C. Rapid and sensitive voltammetric detection of Rhodamine B in chili-containing foodstuffs using $MnO_2$ nanorods/electro-reduced graphene oxide composite. *J. Electrochem. Soc.* **2019**, *166*, B805−B813.

(15) Xu, T.; Fu, L. Y.; Lu, H. Y.; Zhang, M. Y.; Wang, W. L.; Hu, B. N.; Zhou, Y. H.; Yu, G. Electrochemical oxidation degradation of Rhodamine B dye on boron-doped diamond electrode: Input mode of power attenuation. *J. Clean. Prod.* **2023**, *401*, No. 136794.

(16) Baddouh, A.; Bessegato, G. G.; Rguiti, M. M.; El Ibrahimi, B.; Bazzi, L.; Hilali, M.; Zanoni, M. V. B. Electrochemical decolorization of rhodamine B dye: Influence of anode material, chloride concentration and current density. *J. Environ. Chem. Eng.* **2018**, *6*, 2041−2047.
(17) Kothari, M. S.; Shah, K. A. Electrochemical oxidation for decolorization of Rhodamine-B dye using mixed metal oxide electrode: Modeling and optimization. *Water Sci. Technol.* **2020**, *81*, 720−731.
(18) Dai, Q. Z.; Jiang, L.; Luo, X. B. Electrochemical oxidation of Rhodamine B: Optimization and degradation mechanism. *Int. J. Electrochem. Sc.* **2017**, *12*, 4265−4276.
(19) Wu, J.; Zhu, K.; Xu, H.; Yan, W. Electrochemical oxidation of rhodamine B by $PbO_2$/Sb-$SnO_2$/$TiO_2$ nanotube arrays electrode. *Chin. J. Catal.* **2019**, *40*, 917−927.
(20) Wei, Z.; Kang, X. Q.; Xu, S. Y.; Zhou, X. K.; Jia, B.; Feng, Q. Electrochemical oxidation of Rhodamine B with cerium and sodium dodecyl benzene sulfonate co-modified Ti/$PbO_2$ electrodes: Preparation, characterization, optimization, application. *Chin. J. Chem. Eng.* **2021**, *32*, 191−202.
(21) Duan, Y.; Chen, Y.; Wen, Q.; Duan, T. G. Electrodeposition preparation of a cauliflower-like Sb-$SnO_2$ electrode from DMSO solution for electrochemical dye decolorization. *RSC Adv.* **2016**, *6*, 48043−48048.
(22) Man, S. S.; Yin, Z. H.; Zhou, S. B.; Pameté, E.; Xu, L.; Bao, H. B.; Yang, W. J.; Mo, Z. H.; Presser, V.; Li, X. M. Novel Sb-$SnO_2$ electrode with $Ti^{3+}$ self-doped urchin-like rutile $TiO_2$ nanoclusters as the interlayer for the effective degradation of dye pollutants. *ChemSusChem.* **2023**, *16*, No. e202201901.
(23) Maharana, D.; Niu, J. F.; Gao, D.; Xu, Z. S.; Shi, J. H. Electrochemical degradation of Rhodamine B over Ti/$SnO_2$-Sb electrode. *Water Environ. Res.* **2015**, *87*, 304−311.
(24) Wai, T. P.; Yin, Y. L.; Zhang, X.; Li, Z. H. Preparation of Ti/$SnO_2$-Sb/rare earth electrodes containing different contents of Ni intermediate layer for efficient electrochemical decolorization of Rhodamine B. *J. Chem.* **2021**, *2021*, No. 2672674.
(25) Di, J.; Zhu, M.; Jamakanga, R.; Gai, X.; Li, Y.; Yang, R. Electrochemical activation combined with advanced oxidation on $NiCo_2O_4$ nanoarray electrode for decomposition of Rhodamine B. *J. Water. Process. Eng.* **2020**, *37*, No. 101386.
(26) Kim, J.; Yeom, C.; Kim, Y. Electrochemical degradation of organic dyes with a porous gold electrode. *Korean J. Chem. Eng.* **2016**, *33*, 1855−1859.
(27) Zhang, Z. J.; Feng, Y.; Liu, N.; Zhao, Y. H.; Wang, X. W.; Yang, S. M.; Long, Y. Y.; Qiu, L. P. Preparation of Sn/Mn loaded steel slag zeolite particle electrode and its removal effect on Rhodamine B (RhB). *J. Water Process Eng.* **2020**, *37*, No. 101417.
(28) Liu, H. Y.; Ren, M.; Zhang, Z. C.; Qu, J.; Ma, Y.; Lu, N. A novel electrocatalytic approach for effective degradation of Rh-B in water using carbon nanotubes and agarose. *Environ. Sci. Pollut. Res.* **2018**, *25*, 12361−12372.
(29) Berenguer, R.; Sieben, J. M.; Quijada, C.; Morallón, E. Electrocatalytic degradation of phenol on Pt- and Ru-doped Ti/$SnO_2$-Sb anodes in an alkaline medium. *Appl. Catal., B* **2016**, *199*, 394−404.
(30) Li, G. L.; Qi, X. M.; Wu, J. T.; Xu, L. J.; Wan, X.; Liu, Y.; Chen, Y. W.; Li, Q. Ultrasensitive, label-free voltammetric determination of norfloxacin based on molecularly imprinted polymers and Au nanoparticle-functionalized black phosphorus nanosheet nanocomposite. *J. Hazard. Mater.* **2022**, *436*, No. 129107.
(31) Duan, Y.; Chen, Y.; Wen, Q.; Duan, T. Fabrication of dense spherical and rhombic Ti/Sb-$SnO_2$ electrodes with enhanced electrochemical activity by colloidal electrodeposition. *J. Electroanal. Chem.* **2016**, *768*, 81−88.
(32) Song, Y. F.; Liu, J. M.; Ge, F.; Huang, X.; Zhao, Y. Z. Influence of Nd-doping on the degradation performance of Ti/Sb-$SnO_2$ electrode. *J. Environ. Chem. Eng.* **2021**, *9*, No. 105409.
(33) Wu, M. Z.; Lu, L. J.; Yang, Y. B.; Chang, Y.; Chen, R. X.; Li, Y.; Du, J.; Tao, C. Y.; Liu, Z. H.; Liu, Y. J.; Gou, L.; Pan, S. H.; Ran, D.; Li, J. A triethanolamine-assisted fabrication of stable Sb doped-$SnO_2$/Ti electrode for electrocatalytic oxidation of rhodamine B. *Colloid Surface A* **2022**, *634*, No. 127976.
(34) Ganiyu, S. O.; Martínez-Huitle, C. A.; Oturan, M. A. Electrochemical advanced oxidation processes for wastewater treatment: Advances in formation and detection of reactive species and mechanisms. *Curr. Opin. Electrochem.* **2021**, *27*, No. 100678.
(35) Sopaj, F.; Rodrigo, M. A.; Oturan, N.; Podvorica, F. I.; Pinson, J.; Oturan, M. A. Influence of the anode materials on the electrochemical oxidation efficiency. Application to oxidative degradation of the pharmaceutical amoxicillin. *Chem. Eng. J.* **2015**, *262*, 286−294.
(36) Freinbichler, W.; Bianchi, L.; Colivicchi, M. A.; Ballini, C.; Tipton, K. F.; Linert, W.; Della Corte, L. The detection of hydroxyl radicals in vivo. *J. Inorg. Biochem.* **2008**, *102*, 1329−1333.
(37) Xue, J. Q.; Jiang, M.; Yu, L. H.; Luo, Y.; Tang, C. B. Influence of trapping agents on hydroxyI radical detection in electrochemical oxidation system. *J. Anal. Sci.* **2015**, *31*, 606−610. (in Chinese)
(38) Xu, H.; Yan, W.; Tang, C. L. A novel method to prepare metal oxide electrode: Spin-coating with thermal decomposition. *Chin. Chem. Lett.* **2011**, *22*, 354−357.
(39) Zhang, Z. K.; Wang, Z. Y.; Sun, Y. F.; Jiang, S. S.; Shi, L.; Bi, Q.; Xue, J. Q. Preparation of a novel Ni/Sb co-doped Ti/$SnO_2$ electrode with carbon nanotubes as growth template by electrodeposition in a deep eutectic solvent. *J. Electroanal. Chem.* **2022**, *911*, No. 116225.
(40) Grzeta, B.; Tkalcec, E.; Goebbert, C.; Takeda, M.; Takahashi, M.; Nomura, K.; Jaksic, M. Structural studies of nanocrystalline $SnO_2$ doped with antimony: XRD and Mossbauer spectroscopy. *J. Phys. Chem. Solids* **2002**, *63*, 765−772.
(41) Duan, Y.; Wen, Q.; Chen, Y.; Duan, T. G.; Zhou, Y. D. Preparation and characterization of TiN-doped Ti/$SnO_2$-Sb electrode by dip coating for Orange II decolorization. *Appl. Surf. Sci.* **2014**, *320*, 746−755.
(42) Hussain, S.; Jacob, J.; Riaz, N.; Mahmood, K.; Ali, A.; Amin, N.; Nabi, G.; Isa, M.; Mahmood, M. H. R. Effect of growth temperature on catalyst free hydrothermal synthesis of crystalline $SnO_2$ microsheets. *Ceram. Int.* **2019**, *45*, 4053−4058.
(43) Song, Y. F.; Liu, J. M.; Ge, F.; Huang, X.; Zhang, Y.; Ge, H. H.; Meng, X. J.; Zhao, Y. Z. Influence of Nd-doping on the degradation performance of Ti/Sb-$SnO_2$ electrode. *J. Environ. Chem. Eng.* **2021**, *9*, No. 105409.
(44) Man, S. S.; Zhou, S. B.; Yin, Z. H.; Zhang, M.; Sun, Q.; Yang, H.; Xu, K.; Bao, H.; Xu, L.; Yang, W.; Mo, Z.; Li, X. Fabrication of a novel $Ti_3C_2$-modified Sb-$SnO_2$ porous electrode for electrochemical oxidation of organic pollutants. *Sep. Purif. Technol.* **2023**, *306*, No. 122601.
(45) Tang, Y.; Wu, D.; Chen, S.; Zhang, F.; Jia, J.; Feng, X. Highly reversible and ultra-fast lithium storage in mesoporous graphene-based $TiO_2$/$SnO_2$ hybrid nanosheets. *Energy Environ. Sci.* **2013**, *6*, 2447−2451.
(46) Chen, Z.; Jin, Y.; Yang, W.; Xu, B.; Chen, Y.; Yin, X.; Liu, Y. Fabrication and characterization of polypyrrole coatings by embedding antimony modified $SnO_2$ nanoparticles. *J. Ind. Eng. Chem.* **2019**, *75*, 178−186.
(47) Zhao, J.; Chi, Z.; Dong, H.; Sun, C.; Yu, H.; Yu, H. Degradation of desphenyl chloridazon in a novel synergetic electrocatalytic system with Ni-Sb-$SnO_2$/Ti anode and PEDOT/PSS-CNTs modified air diffusion cathode. *J. Clean. Prod.* **2021**, *300*, No. 126961.
(48) Shi, C.; Yu, S.; Li, C. Fabrication of aligned carbon nanofiber doped with $SnO_2$-Sb for efficient electrochemical removal of tetracycline. *Chem. Eng. J.* **2022**, *441*, No. 136052.
(49) Montilla, F.; Morallón, E.; De Battisti, A.; Barison, S.; Daolio, S.; Vázquez, J. L. Preparation and characterization of antimony-doped tin dioxide electrodes. 3. XPS and SIMS characterization. *J. Phys. Chem. B* **2004**, *108*, 15976−15981.
(50) Wu, T.; Zhao, G. H.; Lei, Y. Z.; Li, P. Q. Distinctive tin dioxide anode fabricated by pulse electrodeposition: high oxygen evolution potential and efficient electrochemical degradation of fluorobenzene. *J. Phys. Chem. C* **2011**, *115*, 3888−3898.


https://doi.org/10.1021/acsomega.3c08391
*ACS Omega* 2023, 8, 48480−48490

(51) Fan, W. X.; Wang, A. N.; Wang, L.; Jiang, X.; Xue, Z. Z.; Li, J. H.; Wang, G. M. Hollow carbon nanopillar arrays encapsulated with Pd-Cu alloy nanoparticles for the oxygen evolution reaction. *ACS Appl. Mater. Interfaces* **2023**, *15*, 13600−13608.
(52) Dai, Q.; Xia, Y.; Chen, J. Mechanism of enhanced electrochemical degradation of highly concentrated aspirin wastewater using a rare earth La-Y co-doped $PbO_2$ electrode. *Electrochim. Acta* **2016**, *188*, 871−881.
(53) Sun, Y.; Cheng, S. A.; Yu, Z.; Li, L. X.; Li, C. C.; Yang, J. W. Elucidating deactivation mechanisms of Pd-doped and un-doped Ti/$SnO_2$-Sb electrodes. *J. Alloy. Compd.* **2020**, *834*, No. 155184.
(54) Wu, T.; Zhao, G. H.; Lei, Y. Z.; Li, P. Q. Distinctive tin dioxide anode fabricated by pulse electrodeposition: high oxygen evolution potential and efficient electrochemical degradation of fluorobenzene. *J. Phys. Chem. C* **2011**, *115*, 3888−3898.
(55) Wan, C. L.; Zhao, L. F.; Wu, C. Y.; Lin, L.; Liu, X. $Bi^{5+}$ doping improves the electrochemical properties of Ti/$SnO_2$-Sb/$PbO_2$ electrode and its electrocatalytic performance for phenol. *J. Clean. Prod.* **2022**, *380*, No. 135005.
(56) Xu, T.; Fu, L. Y.; Lu, H. Y.; Zhang, M. Y.; Wang, W. L.; Hu, B. N.; Zhou, Y. H.; Yu, G. Electrochemical oxidation degradation of Rhodamine B dye on boron-doped diamond electrode: Input mode of power attenuation. *J. Clean. Prod.* **2023**, *401*, No. 136794.
(57) Zhou, C. S.; Liu, Z. D.; Fang, L. J.; Guo, Y. L.; Feng, Y. P.; Yang, M. Kinetic and mechanistic study of Rhodamine B degradation by $H_2O_2$ and Cu/$Al_2O_3$/g-$C_3N_4$ composite. *Catalysts.* **2020**, *10*, 317−317.


https://doi.org/10.1021/acsomega.3c08391
*ACS Omega* 2023, 8, 48480−48490